



Tuning magnetotransport properties through chemical substitution in Pr- and Sm-doped NdRuO₃ thin films

Takahiro C. Fujita ,* Shunsuke Senzaki, and Ling-Fei Zhang 

Department of Applied Physics and Quantum-Phase Electronics Center (QPEC), University of Tokyo, Tokyo 113-8656, Japan

Masashi Kawasaki 

Department of Applied Physics and Quantum-Phase Electronics Center (QPEC), University of Tokyo, Tokyo 113-8656, Japan
and Center for Emergent Matter Science (CEMS), RIKEN, Saitama 351-0198, Japan



(Received 10 April 2024; accepted 25 June 2024; published 16 July 2024)

We have investigated the magnetotransport properties for solid-solution thin films of Nd_{1-x}Pr_xRuO₃ and Nd_{1-y}Sm_yRuO₃ prepared through a solid phase epitaxy. It is found that the peculiar magnetotransport properties that emerge in NdRuO₃ are modified by the systematic control of the electron correlation strength through the tuning of the bandwidth as well as in the total angular momentum J of rare earth magnetic ions. The transition from metal to insulator is observed with increasing the concentration y of smaller Sm³⁺ in Nd_{1-y}Sm_yRuO₃, while Nd_{1-x}Pr_xRuO₃ is kept metallic with increasing x for larger Pr³⁺. An anomalous Hall effect is observed for all the conducting samples with the maximum Hall angle appearing for NdRuO₃. The topological Hall effect observed for NdRuO₃ gradually diminishes with increasing the doping concentrations x and y .

DOI: [10.1103/PhysRevMaterials.8.074407](https://doi.org/10.1103/PhysRevMaterials.8.074407)

I. INTRODUCTION

Transition metal perovskite oxide (AMO_3 , M : transition metal) is an intriguing platform for studying the physical properties of strongly correlated electron systems. The intricate interplay between the charge, orbital, and spin degrees of freedom manifests a myriad of emergent phenomena. The interplay between electron correlation (U) and spin-orbit interaction (SOI) has recently attracted considerable attention as an important origin for realizing novel electronic and magnetic phases [1]. In perovskite iridates, the presence of the $J_{\text{eff}} = 1/2$ state for $5d^5$ electrons on Ir⁴⁺ has led to the discovery of various unconventional properties, such as Dirac semimetal for AlIrO₃ [2–4] and spin-orbit Mott-insulator state for Sr₂IrO₄ [5]. Similarly, $4d^5$ electron configuration in Ru³⁺ is of considerable interest, while the SOI is not as strong as in Ir⁴⁺. Indeed, owing to the $J_{\text{eff}} = 1/2$ state, α -RuCl₃ is theoretically proposed to be Kitaev quantum spin liquid [6] and experimentally substantiated through the half-integer thermal quantum Hall effect [7]. In oxides, the stable oxidation state of Ru is generally +4 or higher. $LnRuO_3$ (Ln : lanthanide), which possesses an orthorhombic perovskite structure, represents rare exceptions wherein Ru adopts a +3 oxidation state. Due to the inherent instability of Ru³⁺, however, studies on $LnRuO_3$ have been rather limited to bulk polycrystals [8–11] and single crystals [12]. Consequently, the electronic and magnetic properties of these compounds have not been revealed well, in stark contrast to an immense amount of previous literature dedicated to $AeRu^{4+}O_3$ (Ae : alkaline earth) [13,14].

Recently, we have demonstrated an epitaxial stabilization of LaRuO₃ and NdRuO₃ thin films with a solid phase epitaxy technique and performed comprehensive magnetotransport measurements at ultra-low temperatures down to 50 mK and under high magnetic fields up to 54 T [15]. Despite similarly metallic behaviors in both compounds, magnetotransport properties are quite different, which can be attributed to the distinction between the nonmagnetic La³⁺ and magnetic Nd³⁺ ions. LaRuO₃ is a paramagnetic metal exhibiting a positive magnetoresistance and linear Hall effect down to 50 mK. NdRuO₃, on the other hand, exhibits a nonlinear Hall effect and negative magnetoresistance, as in the case of typical magnetic metals. NdRuO₃ shows an unconventional anomalous Hall effect (AHE), namely, the topological Hall effect (THE), below 1.5 K plausibly originating from the noncoplanar spin texture of Nd³⁺ ions and resultant scalar spin chirality. These findings indicate a crucial role in the transport properties of the f - d exchange interaction between Ln - $4f$ localized moments and Ru- $4d$ itinerant electrons. Additionally, the cooperation between U and SOI may potentially give rise to abundant emergent quantum states as in the case of $Ln_2Ir_2O_7$ [16–18]. To gain further insights, it is a promising way to control magnetic properties and U through the doping on Ln site in $LnRuO_3$.

In this work, we have investigated the magnetotransport properties for solid-solution thin films of Nd_{1-x}Pr_xRuO₃ and Nd_{1-y}Sm_yRuO₃. Starting from NdRuO₃, we have substituted Nd³⁺ with Pr³⁺ or Sm³⁺, where ionic radius and total angular momentum J are Sm³⁺ (1.132 Å, $J = 2.5$), Nd³⁺ (1.163 Å, $J = 4.5$), and Pr³⁺ (1.179 Å, $J = 4$). Chemical substitution is a well-established way to control effective U by modulating the one-electron bandwidth, which is the so-called “chemical pressure effect” [19]. Indeed, the relationship between

*Contact author: fujita@ap.t.u-tokyo.ac.jp

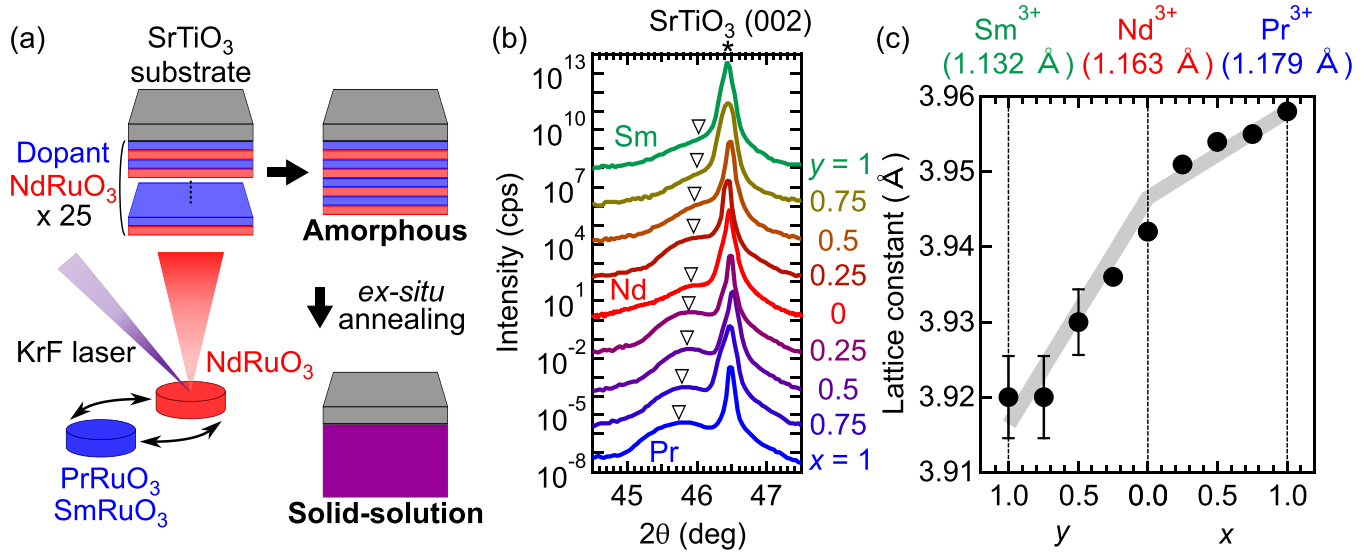


FIG. 1. (a) Schematics of the sample preparation method. Amorphous precursor film is deposited by pulsed laser deposition while switching two targets, and then annealed *ex situ* to obtain a solid-solution epitaxial film with a thickness of ~ 10 nm. (b) X-ray diffraction θ - 2θ scans for $\text{Nd}_{1-x}\text{Pr}_x\text{RuO}_3$ and $\text{Nd}_{1-y}\text{Sm}_y\text{RuO}_3$ films taken around STO (002) peak (vertically shifted for clarity). Peaks from STO substrate and films are marked with an asterisk and triangles, respectively. (c) Out-of-plane lattice spacing d_{001} deduced from the (002) peak position of the films as a function of the nominal doping concentration x and y . Error bars are indicated for Sm-rich films ($y \geq 0.5$) due to the ambiguity of the peak positions.

the bandwidth and the average size of A-site ions has been well studied for perovskite oxides. Therefore, the present solid-solution films based on NdRuO_3 provide an ideal platform to study the bandwidth control effect on its electronic state, and to gain a hint for the origin of the unconventional AHE. We have revealed that the electronic state changes from metal to insulator upon doping smaller Sm^{3+} reminiscent of the Mott transition. Negative magnetoresistance at lower temperatures in NdRuO_3 is enhanced (suppressed) with doping Sm (Pr) and eventually becomes positive for PrRuO_3 . In addition, we have observed the reduction of anomalous Hall angle and the disappearance of the THE on both sides of heavy doping.

II. METHODS

$\text{Nd}_{1-x}\text{Pr}_x\text{RuO}_3$ and $\text{Nd}_{1-y}\text{Sm}_y\text{RuO}_3$ thin films with $x, y = 0, 0.25, 0.5, 0.75, 1$ were fabricated on SrTiO_3 (STO)(001) substrates with a combination of pulsed laser deposition and *ex situ* annealing, following the procedure described in Ref. [15]. Targets for LnRuO_3 layers were prepared by solid-state reaction using Ln_2O_3 ($\text{Ln} = \text{Nd}$ or Sm) or Pr_6O_{11} and RuO_2 powders as chemical agents. To avoid the deficiency of Ru, these powders were mixed with molar ratio of $\text{Ln}:\text{Ru} = 1:1.25$. The mixed powders were milled and calcined for 24 h at 1150°C , forming pyrochlore $\text{Ln}_2\text{Ru}_2\text{O}_7$ phases while excess Ru being remained as RuO_2 . Before deposition, chemically etched STO substrates were annealed *in situ* at 950°C under 10^{-5} Torr oxygen to obtain a clear step-terrace structure with single-unit-cell height [20]. A KrF excimer laser ($\lambda = 248$ nm) with a pulse frequency of 5 Hz and a laser fluence of ~ 2 J/cm² was employed to ablate the targets. By alternately ablating NdRuO_3 and dopant (i.e., PrRuO_3 or SmRuO_3) targets, amorphous multilayer films were first

deposited at a substrate temperature of 600°C and an oxygen pressure of 0.1 mTorr as shown in Fig. 1(a). The doping concentration was controlled by the thickness ratio of two constituent layers. Here it is worth noting that the doping concentrations x and y for $\text{Nd}_{1-x}\text{Pr}_x\text{RuO}_3$ and $\text{Nd}_{1-y}\text{Sm}_y\text{RuO}_3$ in this work are nominal values. Because all three Ln-site elements (Pr, Nd, Sm) are located close to each other on the periodic table, it is unable to determine the actual dopant levels of the films through conventional energy-dispersive x-ray spectroscopy technique. The total thicknesses of the films were designed to be ~ 10 nm, which was confirmed with x-ray reflectivity measurements at a low-angle range. The amorphous films were then annealed *ex situ* with RuO_2 powder at 1000°C for 2 h under 160 ml/min N_2 flow. The annealing process promotes the epitaxial crystallization as well as the formation of a solid solution of the two constituent compounds [Fig. 1(a)].

Figure 1(b) summarizes the x-ray diffraction (XRD) patterns of the $\text{Nd}_{1-x}\text{Pr}_x\text{RuO}_3$ and $\text{Nd}_{1-y}\text{Sm}_y\text{RuO}_3$ films. The films are confirmed to have a (001) oriented single phase in a pseudocubic setting. The clear peak shift indicates that the lattice constant systematically expands (shrinks) upon Pr (Sm) doping. Figure 1(c) shows the out-of-plane lattice spacing d_{001} deduced from the (002) peak position of the films. Note that Sm-rich films ($y \geq 0.5$) have large error bars, because their peak positions are adjacent to the peaks from STO substrate. The deduced d_{001} is almost linear to the nominal doping concentrations x and y , indicating uniformity of the dopants. Coherently strained lattice structure of the films is confirmed by XRD reciprocal space mappings around STO (103) peak (see Supplemental Material, Fig. S1 [21], including Refs. [15,22,23]).

Magnetotransport measurements were performed in a liquid He cryostat with a 9 T superconducting magnet (Physical

Property Measurement System, Quantum Design Co.) down to 0.5 K. Ni (10 nm) and Au (50 nm) bilayer films were deposited by electron beam evaporation as electrodes of a Hall-bar structure fabricated by a scribe. Aluminum wires were attached to the six electrodes to obtain longitudinal resistivity (ρ_{xx}) and Hall resistivity (ρ_{yx}) by the four-terminal measurement method. The magnetic field (B) was applied perpendicularly to the film surface to deduce ρ_{xx} and ρ_{yx} by conventional symmetrization and antisymmetrization procedures, respectively.

III. RESULTS AND DISCUSSION

The temperature (T) dependence of ρ_{xx} for $\text{Nd}_{1-x}\text{Pr}_x\text{RuO}_3$ and $\text{Nd}_{1-y}\text{Sm}_y\text{RuO}_3$ is presented in Figs. 2(a)–2(c). $\text{Nd}_{1-x}\text{Pr}_x\text{RuO}_3$ exhibits an overall metallic behavior accompanied by a slight upturn at lower temperatures as in the case of NdRuO_3 , while the upturn is totally suppressed in PrRuO_3 as can be seen in the magnified Fig. 2(a). In contrast, $\text{Nd}_{1-y}\text{Sm}_y\text{RuO}_3$ shows a systematic transition from metal to insulator upon increasing y . This difference in ρ_{xx} - T curves with chemical substitution shows an implication that the electronic state is systematically shifted from metal in PrRuO_3 to insulator in SmRuO_3 . This is, indeed, consistent with the chemical pressure effects; the larger Ln ion increases the Ru-O-Ru bond angle to suppress effective U and enhance metallic states [19]. We fit the ρ_{xx} - T curves for $\text{Nd}_{1-y}\text{Sm}_y\text{RuO}_3$, assuming a three-dimensional Mott variable-range hopping to confirm the enhanced localization (Supplemental Material, Fig. S2 [21]). Our thin films are strained on the substrate as discussed above (Fig. S1 [21]), thus the films are imposed by not only chemical pressure but also a physical one. Nevertheless, the observed trend in ρ_{xx} - T curves can be explained by the chemical pressure effects, thus U may be responsible for the transport properties in the range of Ln discussed in the present work.

We measured the T dependence of the magnetoresistance ratio under $B = 9$ T ($\text{MRR} \equiv \rho_{xx}(9 \text{ T})/\rho_{xx}(0) - 1$) for the NdRuO_3 , SmRuO_3 , and PrRuO_3 films, as displayed in Fig. 2(d). MRR is almost zero at higher temperatures than ~ 100 K for all compounds, which is followed by positive MRR upon further cooling. As temperature decreases, positive MRR saturates at ~ 10 (~ 20) K for NdRuO_3 (SmRuO_3) and turns negative at lower temperatures. In contrast, positive MRR keeps increasing as one lowers the temperature for PrRuO_3 . We also measured B dependence of MRR at various temperatures (see Supplemental Material, Fig. S3 [21]). This contrasting trend of MRR depending on Ln is of interest as will be discussed later.

We now turn to the Hall effect of the films. Magnetic field dependences of ρ_{yx} are shown in Fig. S4 [21] at various temperatures. As we have reported for NdRuO_3 in Ref. [15], ρ_{yx} starts to contain the anomalous Hall contribution below ~ 100 K, and the ordinary Hall coefficient (R_H) is almost constant below 150 K, which is confirmed by the high field measurements up to 54 T (see Supplemental Material, Fig. S5 [21]). Therefore, by assuming that R_H is constant below 150 K, ρ_{AHE} is calculated by $\rho_{\text{AHE}}(B) \equiv \rho_{yx}(B) - R_H(150 \text{ K})B$ for the present solid-solution films as displayed in Fig. 3. Here the data at 0.5 (black) and 3 K (blue) are shown

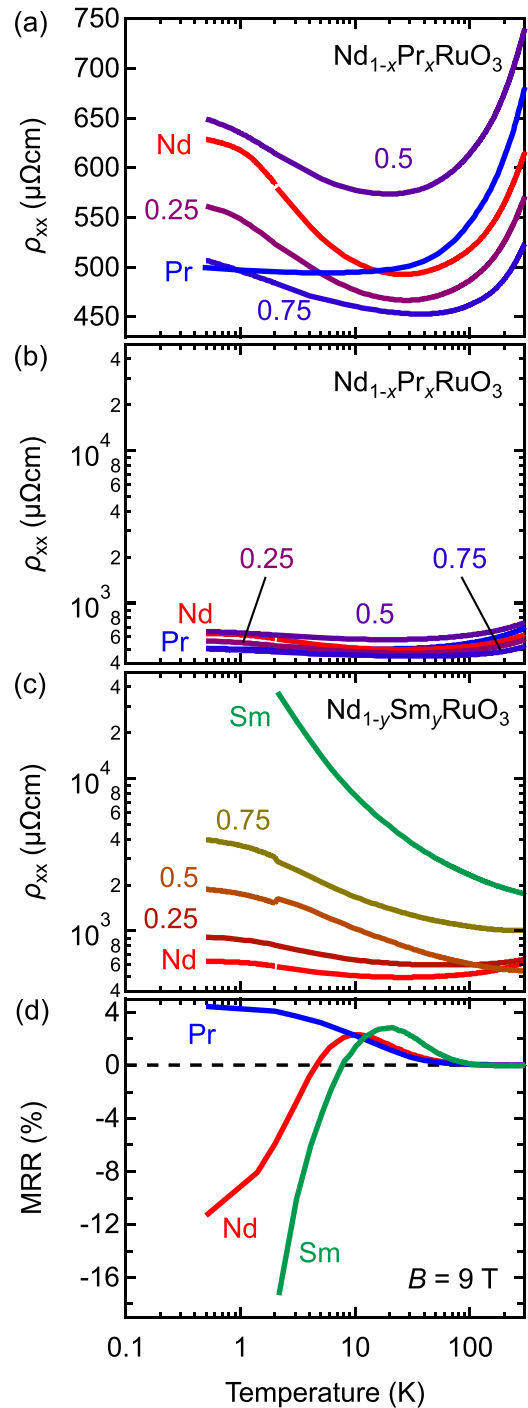


FIG. 2. Temperature dependence of longitudinal resistivity (ρ_{xx}) for (a), (b) $\text{Nd}_{1-x}\text{Pr}_x\text{RuO}_3$ and (c) $\text{Nd}_{1-y}\text{Sm}_y\text{RuO}_3$ films. The vertical axis is in linear scale in panel (a) and the logarithmic scales for panels (b) and (c). (d) Temperature dependence of magnetoresistance ratio under $B = 9$ T [$\text{MRR} \equiv \rho_{xx}(9 \text{ T})/\rho_{xx}(0) - 1$] for PrRuO_3 , NdRuO_3 , and SmRuO_3 films.

to discuss the low-temperature behavior, where the f - d interaction is more prominent. Because of the increasing ρ_{xx} as shown in Fig. 2(c), the data become noisy for Sm-rich films ($y = 0.5, 0.75, 1$), especially at 0.5 K. The measurement at 0.5 K was even not possible for films with $y = 0.75, 1$. All the films exhibit nonlinear ρ_{yx} as expected for AHE. NdRuO_3 has been

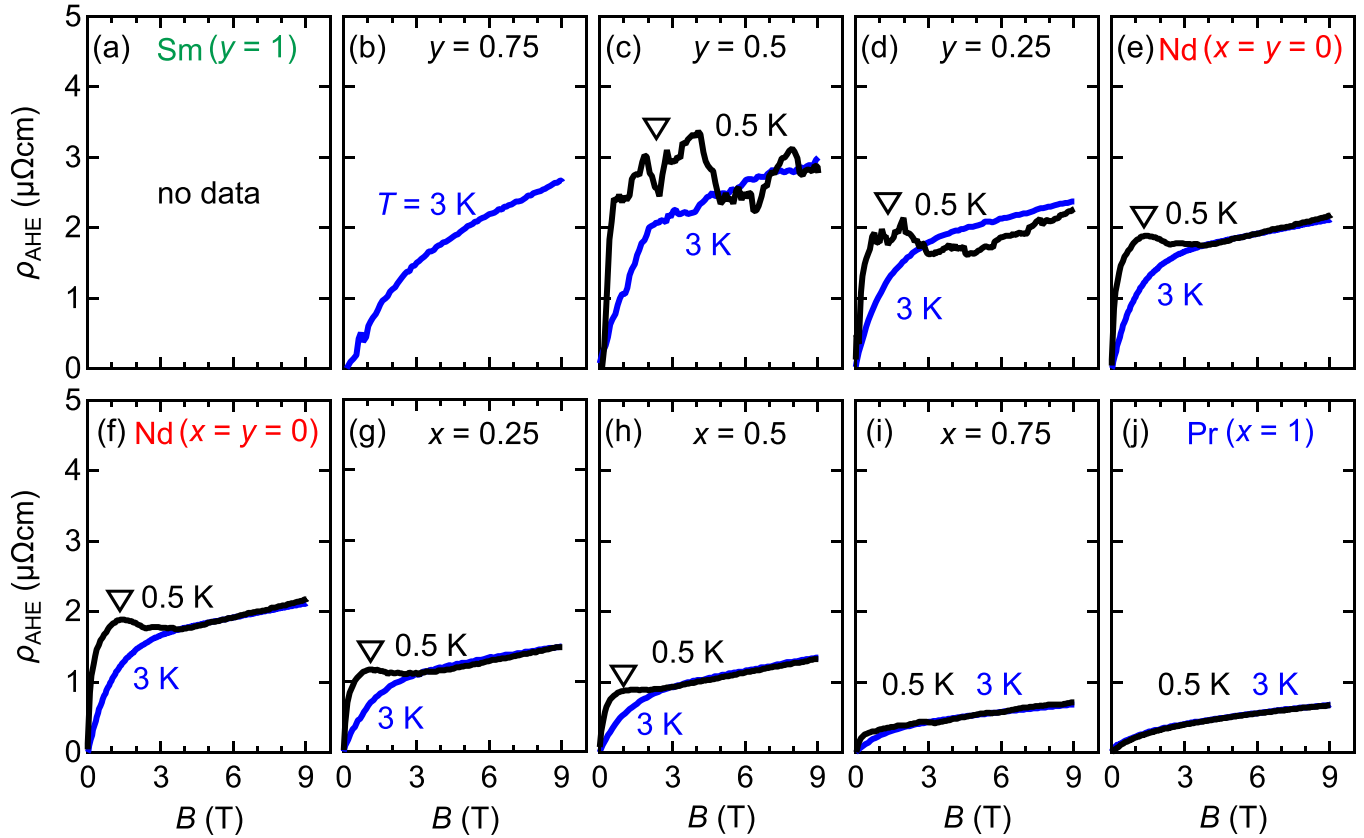


FIG. 3. (a) Magnetic field dependence of anomalous Hall resistivity (ρ_{AHE}) at low temperatures for (a)–(e) $\text{Nd}_{1-y}\text{Sm}_y\text{RuO}_3$ and (f)–(j) $\text{Nd}_{1-x}\text{Pr}_x\text{RuO}_3$ thin films. The hump structure characteristic of the topological Hall effect (see text) is denoted by the triangles. Note that the data in panels (e) and (f) are identical, and that data at 0.5 and 3 K are overlapped in panel (j).

revealed to exhibit THE below ~ 1 K due to a noncoplanar spin texture realized during the magnetic transition, which is indicated by the triangles in Figs. 3(e) and 3(f). The unique hump structures at around $B = 1$ T originating from THE seemingly remain for $x, y \leq 0.5$ [Figs. 3(c)–3(h)] although the data are noisy in the Sm-doped side. In particular for Pr-rich films ($x = 0.75, 1$) in Figs. 3(i)–3(j), THE is indiscernible. At the same time, the kink structure in MRR observed for NdRuO_3 also disappears with increasing x and y (see Supplemental Material, Fig. S6 [21]), indicating that these two features are attributed to the same origin: plausibly a sort of magnetic transition.

To quantitatively discuss the magnetotransport properties, the data are summarized in Fig. 4 for (a) ρ_{xx} , (b) MRR, and (c) anomalous Hall angle ($\theta_{\text{AHE}} \equiv \rho_{xx}\rho_{\text{AHE}}/(\rho_{xx}^2 + \rho_{\text{AHE}}^2)$) at $B = 9$ T deduced from the transport results (Figs. 2 and 3). Pr doping does not cause appreciable effects on ρ_{xx} . Upon doping Sm, ρ_{xx} systematically increases both at 3 and 300 K; especially for SmRuO_3 , $\rho_{xx}(3 \text{ K})$ diverges and is one order of magnitude higher than $\text{Nd}_{1-x}\text{Pr}_x\text{RuO}_3$ [Fig. 4(a)]. The lattice distortion of perovskite AMO_3 is governed by the tolerance factor f , which is defined as $f = (r_A + r_O)/\sqrt{2}(r_M + r_O)$. Here r_i ($i = A, M, \text{ or } O$) represents the ionic size of each element [24]. When f is close to 1, the cubic perovskite structure is realized. As r_A or equivalently f decreases, the lattice structure distorts to an orthorhombic structure, to which LnRuO_3 belongs [10]. In the case of the orthorhombic lattice, the M - O - M bond angle varies continuously with f ,

regardless of the species of A and M [25,26]. The smaller f indicates the larger bond angle distortion, leading to the reduction of one-electron bandwidth or electron conductivity [19]. In the present system, with using the ionic size of Ln^{3+} and Ru^{3+} , f is calculated as 0.859 (SmRuO_3), 0.870 (NdRuO_3), and 0.875 (PrRuO_3); thus the observed trend is reasonably understood in the framework of a bandwidth-control driven Mott transition.

As shown in Fig. 2(d), the T dependence of MRR for SmRuO_3 and NdRuO_3 contrasts with that of PrRuO_3 especially at lower temperatures. This tendency is further confirmed for the solid-solution films as shown in Fig. 4(b). MRR of NdRuO_3 is negative at both 3 and 0.5 K while the magnitude is larger at 0.5 K. With increasing Pr-doping concentration x , negative MRR is suppressed and turns into positive at both 3 and 0.5 K for PrRuO_3 , the magnitude of which is $\sim 4\%$. In contrast, with increasing Sm-doping concentration y , negative MRR is enhanced, the magnitude of which reaches as much as -25% for $y = 0.5$ at 0.5 K. Considering that all the Ln ions employed in this work are magnetic with finite J , the observed positive MRR in PrRuO_3 is unusual since negative MRR is expected due to the suppression of magnetic scattering by the applied field. Indeed, in the case of LnNiO_3 thin films, negative MRR has been commonly observed for $\text{Ln} = \text{Sm}$ [27], Nd [28], and Pr [29] at lower temperatures, where they are in antiferromagnetic insulating phases. This positive MRR in PrRuO_3 may be related to the emergence of a topological semimetallic state, similar to that

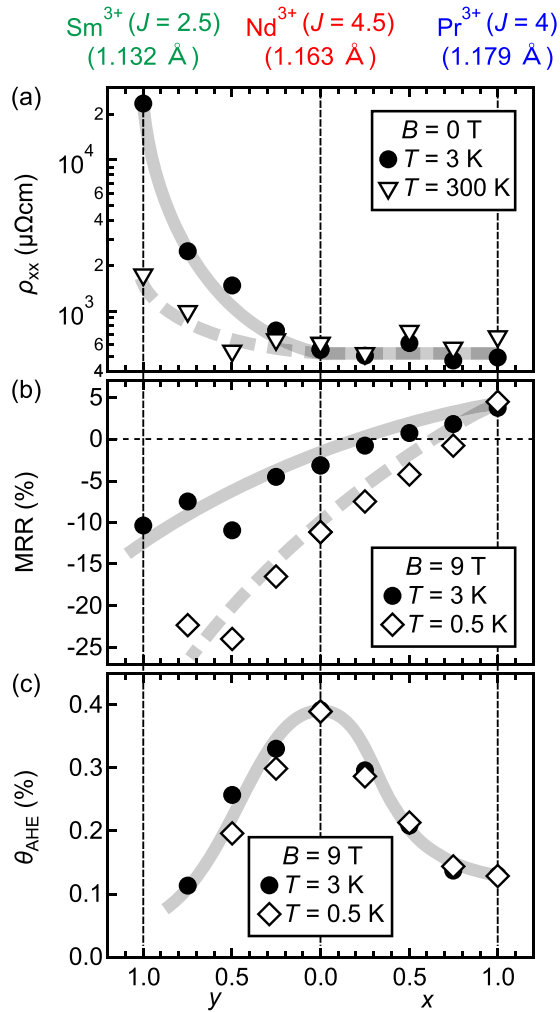


FIG. 4. (a) Longitudinal resistivity (ρ_{xx}) at 3 K and 300 K under $B = 0$ T, (b) MRR at 3 K and 0.5 K under $B = 9$ T, and (c) anomalous Hall angle at 3 K and 0.5 K under $B = 9$ T, as a function of the nominal doping concentrations x and y . On the top, total angular momentum (J) and ionic radii of each Ln^{3+} are also shown. Note that data at 0.5 and 3 K are overlapped for $x = 1$.

observed in SrIrO_3 with large positive MRR [30], which originates from the d^5 electronic configuration of Ir^{4+} . Although PrRuO_3 also possesses d^5 electronic configuration, further

experimental and theoretical investigations are required to validate this analogy.

The anomalous Hall angle is $\sim 0.3\%$ for NdRuO_3 and decreases for both $\text{Nd}_{1-x}\text{Pr}_x\text{RuO}_3$ and $\text{Nd}_{1-y}\text{Sm}_y\text{RuO}_3$ with similar doping concentration dependences [Fig. 4(c)]. At the same time, the feature of THE diminishes as shown in Fig. 3, as well as the kink structure in MRR (Fig. S6 [21]). Due to the small volume and low ordering temperature, it is currently not feasible to perform magnetization measurements for the films to gain further insights and compare them with the observed transition in AHE and THE. One possible reason may be the difference in ordering temperatures of Ln^{3+} spins as THE in this system appears to be related to the spin texture of the Ln site. Indeed, the ordering temperature of Ln^{3+} spins has been reported to remarkably vary depending on Ln in other $Ln\text{MO}_3$ systems such as $M = \text{Cr}, \text{Mn}, \text{Fe}$ [31]. However, additional studies are desired to unambiguously clarify its origin, which is indeed challenging and we wish to see as future work.

IV. CONCLUSION

In summary, we have clarified the magnetotransport properties of $\text{Nd}_{1-x}\text{Pr}_x\text{RuO}_3$ and $\text{Nd}_{1-y}\text{Sm}_y\text{RuO}_3$ thin films. At both ends of the solid solutions, PrRuO_3 and SmRuO_3 respectively show metallic and insulating temperature dependences of ρ_{xx} , implying the transition of the electronic ground state. AHE is consistently observed across the entire range of doping concentrations, while the Hall angle decays and THE disappears on both sides of the doping from NdRuO_3 . Our work on systematic chemical substitution on the novel materials platform of perovskite oxide with Ru^{3+} not only enables the systematic tuning of transport properties but also paves the way for investigating electronic phase transition and potentially uncovering more exotic transport phenomena associated with magnetic topological materials.

ACKNOWLEDGMENTS

This work was supported by JSPS Grants-in-Aid for Scientific Research (S) No. JP22H04958, JSPS Grant-in-Aid for Early-Career Scientists No. JP20K15168, the Mitsubishi Foundation, the Izumi Science and Technology Foundation, the Tokuyama Science Foundation, and the Toyota Physical and Chemical Research Institute.

- [1] W. Witczak-Krempa, G. Chen, Y. B. Kim, and L. Balents, *Annu. Rev. Condens. Matter Phys.* **5**, 57 (2014).
- [2] M. A. Zeb and H.-Y. Kee, *Phys. Rev. B* **86**, 085149 (2012).
- [3] Y. F. Nie, P. D. C. King, C. H. Kim, M. Uchida, H. I. Wei, B. D. Faeth, J. P. Ruf, J. P. C. Ruff, L. Xie, X. Pan, C. J. Fennie, D. G. Schlom, and K. M. Shen, *Phys. Rev. Lett.* **114**, 016401 (2015).
- [4] J. Fujioka, R. Yamada, M. Kawamura, S. Sakai, M. Hirayama, R. Arita, T. Okawa, D. Hashizume, M. Hoshino, and Y. Tokura, *Nat. Commun.* **10**, 362 (2019).
- [5] B. J. Kim, H. Jin, S. J. Moon, J.-Y. Kim, B.-G. Park, C. S. Leem, J. Yu, T. W. Noh, C. Kim, S.-J. Oh, J.-H. Park, V. Durairaj, G. Cao, and E. Rotenberg, *Phys. Rev. Lett.* **101**, 076402 (2008).
- [6] H.-S. Kim, V. Vijay Shankar, A. Catuneanu, and H.-Y. Kee, *Phys. Rev. B* **91**, 241110(R) (2015).
- [7] Y. Kasahara, T. Ohnishi, Y. Mizukami, O. Tanaka, S. Ma, K. Sugii, N. Kurita, H. Tanaka, J. Nasu, Y. Motome, T. Shibauchi, and Y. Matsuda, *Nature (London)* **559**, 227 (2018).
- [8] R. J. Bouchard and J. F. Weiher, *J. Solid State Chem.* **4**, 80 (1972).
- [9] T. Sugiyama and N. Tsuda, *J. Phys. Soc. Jpn.* **68**, 3980 (1999).
- [10] A. Sinclair, J. A. Rodgers, C. V. Topping, M. Mířek, R. D. Stewart, W. Kockelmann, J.-W. G. Bos, and J. P. Attfield, *Angew. Chem., Int. Ed.* **53**, 8343 (2014).

- [11] K. Ji, A. Paul, E. Solana-Madruga, A. M. Arevalo-Lopez, U. V. Waghmare, and J. P. Attfield, *Phys. Rev. Mater.* **4**, 091402(R) (2020).
- [12] B. K. Patel, M. T. K. Kolambage, C. D. McMillen, and J. W. Kolis, *J. Cryst. Growth* **602**, 126979 (2023).
- [13] G. Koster, L. Klein, W. Siemons, G. Rijnders, J. S. Dodge, C.-B. Eom, D. H. A. Blank, and M. R. Beasley, *Rev. Mod. Phys.* **84**, 253 (2012).
- [14] J.-G. Cheng, J.-S. Zhou, and J. B. Goodenough, *Proc. Natl. Acad. Sci. USA* **110**, 13312 (2013).
- [15] L. Zhang, T. C. Fujita, Y. Masutake, M. Kawamura, T.-h. Arima, H. Kumigashira, M. Tokunaga, and M. Kawasaki, *Commun. Mater.* **5**, 35 (2024).
- [16] K. Ueda, J. Fujioka, C. Terakura, and Y. Tokura, *Phys. Rev. B* **92**, 121110(R) (2015).
- [17] Z. Tian, Y. Kohama, T. Tomita, H. Ishizuka, T. H. Hsieh, J. J. Ishikawa, K. Kindo, L. Balents, and S. Nakatsuji, *Nat. Phys.* **12**, 134 (2016).
- [18] B. Cheng, T. Ohtsuki, D. Chaudhuri, S. Nakatsuji, M. Lippmaa, and N. P. Armitage, *Nat. Commun.* **8**, 2097 (2017).
- [19] M. Imada, A. Fujimori, and Y. Tokura, *Rev. Mod. Phys.* **70**, 1039 (1998).
- [20] M. Kawasaki, K. Takahashi, T. Maeda, R. Tsuchiya, M. Shinohara, O. Ishiyama, T. Yonezawa, M. Yoshimoto, and H. Koinuma, *Science* **266**, 1540 (1994).
- [21] See Supplemental Material at <http://link.aps.org/supplemental/10.1103/PhysRevMaterials.8.074407> for XRD reciprocal space mappings of the samples; the variable range hopping analysis for the Sm-doped samples; the magnetic field dependence of magnetoresistance and Hall resistivity; high field measurements data for NdRuO₃; the analysis for the correlation between magnetoresistance and the topological Hall effect.
- [22] N. F. Mott, *J. Non-Cryst. Solids* **1**, 1 (1968).
- [23] B. I. Shklovskii and A. L. Efros, in *Variable-Range Hopping Conduction*, edited by B. I. Shklovskii and A. L. Efros, Springer Series in Solid-State Sciences (Springer, Berlin, 1984), pp. 202–227.
- [24] J. B. Torrance, P. Lacorre, A. I. Nazzari, E. J. Ansaldo, and C. Niedermayer, *Phys. Rev. B* **45**, 8209 (1992).
- [25] M. Marezio, J. P. Remeika, and P. D. Dernier, *Acta Crystallogr., Sect. B* **26**, 2008 (1970).
- [26] D. A. MacLean, H.-N. Ng, and J. E. Greedan, *J. Solid State Chem.* **30**, 35 (1979).
- [27] K. Ramadoss, N. Mandal, X. Dai, Z. Wan, Y. Zhou, L. Rokhinson, Y. P. Chen, J. Hu, and S. Ramanathan, *Phys. Rev. B* **94**, 235124 (2016).
- [28] A. Stupakov, O. Pacheroova, T. Kocourek, M. Jelinek, A. Dejneka, and M. Tyunina, *Phys. Rev. B* **99**, 085111 (2019).
- [29] D. D. K., A. Singh, S. Sathapathy, K. K. Maurya, P. K. Siwach, V. K. Malik, S. S. Kushvaha, and H. K. Singh, *J. Supercond. Novel Magn.* **36**, 623 (2023).
- [30] J. Fujioka, T. Okawa, A. Yamamoto, and Y. Tokura, *Phys. Rev. B* **95**, 121102(R) (2017).
- [31] E. Bousquet and A. Cano, *J. Phys.: Condens. Matter* **28**, 123001 (2016).